Medical Imaging Process & Technology (2023) Volume 6 Issue 1
doi: 10.24294/mipt.v6i1.2719

CASE REPORT

Topographic mapping of oxygen extraction and cerebral venous blood volume fraction in Brain tumors using quantitative BOLD: A case report

Arun Raj T.[1], Karthik K.[2], Joseph Suresh Paul[3,*]

[1] *School of Electronics Systems and Automation, Kerala University of Digital Sciences Innovation & Technology, Trivandrum 695317, India*

[2] *Department of Neuro Imaging, National Institute of Mental Health Neurosciences, Bengaluru 560029, India*

[3] *School of Informatics, Kerala University of Digital Sciences Innovation & Technology, Trivandrum 695317, India*

*** Corresponding author:** Joseph Suresh Paul, j.paul@duk.ac.in

ABSTRACT

Background: While oxygen extraction fraction (OEF) reflects the underlying variations in cerebral brain oxygen metabolism, tissue voxels having elevated volume fraction of blood vessel network with deoxygenated blood, will apparently contribute to higher cerebral venous blood volume fraction (CVBVF). This Case report examines the difference in intra and peri-tumoral topographical patterns of OEF and CVBVF in cases of a meningioma tumor (Case-I) and a low- grade glioma (Case-II). **Methods:** Using a "static dephasing regime" BOLD model, we use the BOLD signal model containing parameters representing OEF and CVBVF. For each voxel in the region of interest, the parameters are solved by non-linearly fitting the signal model using paired differences between logarithms of the measured echo signal after inhomogeneity correction. **Results:** OEF and CVBVF maps in Case-I reveals an interesting phenomenon in the peritumoral parenchyma showing reduced OEF and increased CVBVF levels. The uniformly low CVBVF and elevated OEF in Case-II indicates that even with less density of vasculature, the region extracts higher amount of oxygen. **Conclusion:** While topographic mapping using qBOLD revealed elevated levels of intra-tumoral OEF for both cases, the pattern of CVBVF variation was uniformly low in Case-II.

Keywords: meningioma tumor; glioma; oxygen extraction fraction; venous cerebral blood volume fraction; multi-echo GRE; qBOLD

ARTICLE INFO

Received: 4 September 2023
Accepted: 22 September 2023
Available online: 25 December 2023

1. Introduction

Oxygen extraction fraction (OEF) is a physiological biomarker reflecting the percentage of oxygen extracted from the blood supply, which is directly associated with cerebral metabolism[1]. With varying oxygen demand in tumor cells, OEF can also provide information about the discrepancies in cerebral blood supply. Also given that the tumor cells respond differently towards decreased oxygenation leading to cell death or cell survival, may further lead to the discrepancy in the OEF range[2–6]. The wide variation of tumor oxygenation, coupled with the heterogeneities in the volumetric distribution of the venous blood vessel network is indicated by the cerebral venous blood volume fraction (CVBVF)[6,7].

Failure of vasculature in brain tumors to maintain oxygen levels will correspondingly result in increased OEF to maintain tissue oxygen metabolism. Tumors are well adapted to grow and expand in this oxygen-depleted tumour micro-environment. When there is not

enough blood flow to an area, oxygen does not reach the cells, then OEF is increased with reduced cerebral blood flow. This implies that a major proportion of the tumour tissue might be sufficiently perfused to match its metabolic demands for oxygen and that the OEF analysis provides better discrimination between tumour and the surrounding tissues.

Intracranial meningioma tumors and high-grade gliomas are generally observed to have variable degrees of vascularity[8] with possible presence of tumor cell aggregation, necrosis and edema. Generally, these are slowly growing, with the growth rate at least partly dependent on the ability of the tumour tissues to adapt to variations in oxygen availability following vascularization. The vascular network within the tumor has been observed to have an impact on both Oxygen Extraction Fraction (OEF) and Cerebral Blood Volume Fraction (CVBVF) in the adjacent ipsilateral cortex[9–11].

The qBOLD method is based on the principle that the magnetic susceptibility of blood changes with its oxygenation level. This change affects the MRI signal and can be used to infer the OEF in tissues. The acquired MRI data is then used to fit mathematical models that describe the relationship between the observed signal and the underlying tissue properties, including OEF. These models often consider factors like blood volume, oxygenation levels, and the magnetic susceptibility of blood. Therefore, an investigation into the differences in the spatial patterns of OEF and CVBVF are essential for evaluation of different tumor sub types. As for the current standards, PET with O tracers is the reference standard for quantitative mapping of OEF[12]. In contrast to this, with MRI acquisition, tissue cerebral oxygen consumption is estimated from the susceptibility difference between paramagnetic deoxy-heme in the vasculature and the tissue parenchyma. Whereas echo planar imaging (EPI) is perfumed in diffusion, perfusion and functional imaging due to its ability to image rapid physiologic processes of the human body[13–15].

Numerous approaches have been suggested for the estimation of these topographic maps by employing quantitative modelling of either MRI magnitude or phase data. Among the magnitude modelling techniques are Quantitative Imaging of Extraction of Oxygen and Tissue Consumption (QUIXOTIC)[16], calibrated fMRI[17-20], and Quantitative BOLD (qBOLD)[21,22]. Phase modelling methods have been employed in the context of whole-brain measurements of cerebral metabolic rate of oxygen consumption[23,24].

This case report showcases how qBOLD is used to spatially distinguish metabolic states within both the tumor and its neighbouring area. By analysing various qBOLD parameters, including OEF and CVBVF, we uncovered distinct patterns of cellular density and vascular distribution in a meningeal tumor. Additionally, in the case of low-grade glioma, we consistently observed a region with significantly reduced CVBVF, which is indicative of hypoperfusion.

2. Materials and methods

2.1. Patients

The radiological data included in this case report are taken from participants who underwent MRI scan as part of a retrospective study, approved by the hospital ethics committee at the National Institute for Mental Health and Neuro Sciences (NIMHANS, Bangalore, India). Here, we discuss two cases of which Case-1 corresponds to a subject having left parafalcine meningioma with invasion and mass effects. Case-II corresponds to a subject having right frontal glioma, characterized with minimal mass effect.

2.2. Data acquisition

T1-weighted, T2-weighted, DWI, ASL, and four-echo 3D GRE sequences were implemented on a 3.0 T MRI scanner (Ingenia 3.0 T, Philips, Netherlands) with a 32-channel head array coil. SWI images were reconstructed using the GRE magnitude and phase images. The details of each sequence are as follows:

1) 3D GRE: Initial *TE* = 7.2 ms, Echo spacing = 4.1 ms, *TR* = 31 ms; flip angle = 20°, *FA* = 20°, slice thickness 2.0 mm, acquisition matrix 384 × 325 × 140, Acquisition voxel size: 0.6 × 0.6 × 2 mm, Reconstruction matrix: 672 × 672 × 140, Reconstruction voxel size: 0.3 × 0.3 × 2 mm, *BW* = 300 Hz/pixel and *FOV* = 230 × 189 × 140 mm^3.
2) DWI: *TE* = 86 ms; *TR* = 4480 ms; voxel size: 2.0 × 2.0 × 2.0 mm, Reconstruction matrix: 112 × 110 × 72, and *FOV* = 224 × 224 × 144 mm^3.
3) ASL: *TE* = 13.5 ms; *TR* = 4400 ms; voxel size: 3.0 × 3.0 × 7.0 mm, Reconstruction matrix: 80 × 78 × 19, and *FOV* = 230 × 240 × 133 mm^3.
4) T1W: *TE* =2.3 ms; *TR* = 310.7 ms; flip angle = 30°; voxel size: 2.0 × 2.0 × 2.0 mm, Reconstruction matrix: 256 × 256 × 72, and *FOV* = 224 × 224 × 144 mm^3.
5) T2W: *TE* =80 ms; *TR* = 3112 ms; flip angle = 90°; voxel size: 0.50 × 0.37 × 2.00 mm, Reconstruction Matrix: 480 × 485 × 40, and *FOV* = 230 × 181 × 80 mm^3.

2.3. OEF computation

The quantitative BOLD (qBOLD) model focuses on the signal decay in the "extravascular" space due to the local field inhomogeneities induced by the paramagnetic deoxyhemoglobin in the vessel network. Using a "static dephasing regime" BOLD model in which the vessels are considered to be an ensemble of randomly oriented cylinders[25], we use the BOLD signal model containing parameters representing OEF (Q) and CVBVF (ν). The OEF is computed from the characteristic dephasing time (t_c) in the static dephasing regime[26]. Considering the deviation from a linear exponential decay for the extravascular signal to be negligible for $t > 1.5t_c$, the decaying GRE signal is expressed in terms of a simplified two-exponential decay model representative of a cellular component $\exp(-R_2 t)$, BOLD contribution $F_s(\nu, t_c)$ and the macroscopic inhomogeneities $F(t)$ as[21],

$$S(t) = S_0 \exp(-R_2 t)\, F_s(\nu, t_c) F(t) \tag{1}$$

where $F_s(\nu, t_c) \cong \exp\left[0.3\,\nu \left(\frac{t}{t_c}\right)^2\right]$. We use the Voxel Spread Function (VSF)[27,28] method to estimate $F(t)$, which enables the quantification of tissue-specific effective transverse relaxation rates, holds the potential to give rise to novel MRI biomarkers that can serve as proxies for tissue biological characteristics. These biomarkers may parallel the role of the widely employed longitudinal and transverse relaxation rate constants in MRI clinical research. Using paired differences between logarithms, denoted by *L*, of the measured signal after inhomogeneity correction, we arrive at the modified qBOLD model with elimination of S_0.

For each echo pair, this log difference model is given by

$$L_{i,i+1} = \log(S_i) - \log(S_{i+1}) \tag{2}$$

This is solved as an unconstrained minimization problem by minimizing the cost function

$$J = \underset{R_2,\nu,t_c}{\operatorname{argmin}} \left\| \mathrm{L} - \left[R_2 \Delta\mathrm{T} + \frac{0.3\nu}{t_c^2} \Delta^2\mathrm{T} \right] \right\|_2^2 \tag{3}$$

where $L = \left[L_{1,2}, L_{2,3}, L_{3,4}\right]'$, $\Delta\mathrm{T} = [t_2 - t_1, t_3 - t_2, t_4 - t_3]'$ and $\Delta^2\mathrm{T} = \left[{t_2}^2 - {t_1}^2, {t_3}^2 - {t_2}^2, {t_4}^2 - {t_3}^2\right]'$ for the Multi-echo GRE data (4-echo data). We employed the "fminunc" solver in MATLAB (MathWorks, Natick, MA) to tackle the non-linear optimization problem outlined in Equation (3). This solver is used to find the minimum of unconstrained multivariable functions. We found that the optimization routine consistently yielded stable solutions across a broad range of initial parameter values, ranging from zero to one.

3. Results

MRI data for a 49-year-old male patient with left parafalcine meningioma (Case-1), a 37-year-old male patient with low-grade right frontal glioma (Case-II) and a 43-year-old normal subject are obtained from a 3.0 T scanner (Ingenia 3.0 T, Philips, Netherlands) at the National Institute for Mental Health and Neuro Sciences

(NIMHANS, Bangalore, India). The left-to-right panels of **Figure 1** show the representative Axial SWI, T2W and DWI MRI images of a cortical slice in a meningioma tumor (Case-I) (a1–c1) and glioma (Case-II) (a2–c2).

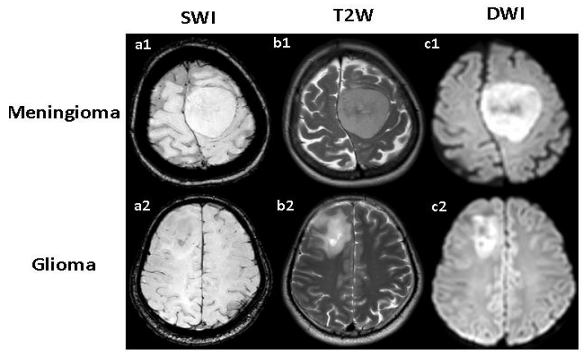

Figure 1. Left-to-right panels show SWI, T2W and DWI images of an axial cortical slice in a meningioma tumor (Case-I) (a1–c1) and glioma (Case-II) (a2–c2).

Case-I revealed Left frontal parasagittal extra axial lesion measuring 5.4 × 4.7 cm in the precentral region with midline shift of ~4 mm. The lesion was isointense to contralateral grey matter on T2W and T1W images. Absence of focus of blooming on SWI was nonsuggestive of intra-tumoral micro-haemorrhages. Dense cellularity of the tumour and absence of perilesional edema was revealed by the restricted diffusion patterns seen in the DWI image. Other imaging features included well-defined lesion outline, absence of peritumoral cysts and perilesional edema.

Case-II revealed Right superior frontal parasagittal intra-axial lesion measuring 4.8 × 3.7 cm involving superior medial frontal and middle frontal gyrus. The lesion was hyperintense on T2W image, hypointense on T1W image, showing no focus of blooming on SWI. DWI showed a few areas of subtle restriction, suggesting mild cellularity. ASL perfusion maps revealed no evidence of hyper-perfusion within the lesion. The overall features conformed to a low-grade glioma.

The left-to-right panels of **Figure 2** shows the skull-stripped T1W magnitude image, OEF and CVBVF maps for the cortical slices in **Figure 1**. Row-wise panels show maps of an age-matched normal subject (a1-c1), Case-I (a2–c2) and Case-II (a3–c3).

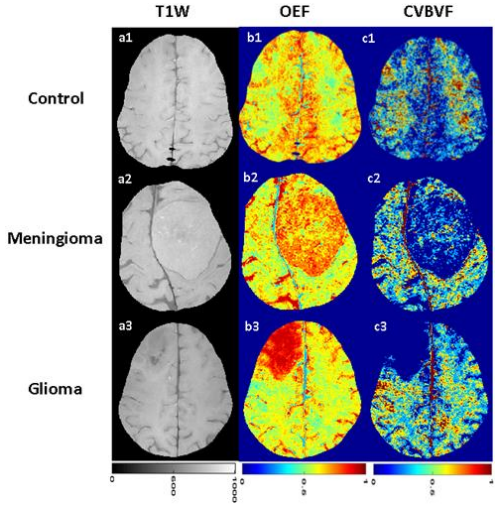

Figure 2. Left-to-right panels show the skull-stripped T1W magnitude image, OEF and CVBVF maps for the cortical slices in Figure 1. Row-wise panels show maps of an age-matched normal subject (a1–c1), Case-I (a2–c2) and Case-II (a3–c3).

Case-I revealed elevated OEF level within the lesion and reduced CVBVF in the periphery compared to the contralateral white matter. The centre demonstrated a few areas of increased CVBVF. This pattern likely

reveals a dense distribution of vascular networks between the center and periphery of the lesion. Due to compressive effect of the tumor on the adjacent parenchyma, the peritumoral parenchyma showed decreased OEF and increased CVBVF.

While Case-II also revealed intra-lesion OEF levels 20%–25% larger than Case-I, a main difference is that the CVBVF map showed topographically uniform and low values. This is in concurrence with the ASL perfusion maps denoting relative hypoperfusion in Case-II. In contrast to Case-I, the combined features from OEF and CVBVF are suggestive of increased metabolism in the tumor having poorly vascularized regions.

4. Discussion

Meningioma tumors and high-grade gliomas are characterised by variable vascular networks, ranging from sparse to highly dense angiogenic subtype[29]. Generally, hyper vascularity provides excess of oxygenated blood and diminishes the demands of oxygen intake[30,31]. CVBVF exhibits non-uniform patterns reflecting heterogeneous composition of aggregated tumor cells. In contrast, the topographic pattern of CVBVF in the low-grade gliomas is found to be uniformly low. Areas with high CVBVF and OEF can ideally correspond to metabolically active portions of the tumor cell aggregations.

The energy metabolism of tumorous tissues is characteristically different from that of the healthy tissue. Recent studies using PET have demonstrated the pathophysiology of intracranial tumours and evaluated the relationship between tumour oxygenation versus metabolism in ipsilateral and contralateral brain regions[32]. The intracranial tumor vasculature is often found to be interconnected with declined oxygen metabolism and cerebral venous blood flow in the overlying ipsilateral cortex, as compared to the contralateral cortical tissue [9–11]. However, the discrepancy and lack of consistency between oxygenation and tumor vasculature has already been well established. Tumour cells respond differently towards decreased oxygenation, leading to cell death or cell survival which may further lead to the discrepancy in the OEF range[3–5].

The blood oxygenation level-dependent (BOLD) contrast, based on changes in the ratio oxyhaemoglobin/deoxyhaemoglobin that exhibit different magnetic properties, opened up the possibility to use this effect to study brain hemodynamic and oxygen consumption by means of MRI measurements[26]. qBOLD can be used for the evaluation of OEF. A combination of the measurement of OEF and the cerebral blood flow allows an evaluation to be made of the cerebral metabolic rate of oxygen consumption[6,33]. It can also be used to measure oxygen tissue saturation in the brain[34].

Case-I represents a tumor characterized by high cellularity without necrosis. OEF and CVBVF maps in Case-I reveals an interesting phenomenon in the peritumoral parenchyma showing reduced OEF and increased CVBVF levels. The uniformly low CVBVF and elevated OEF in Case-II indicates that even with less density of vasculature, the region extracts higher amount of oxygen. This is indicative of hypo-perfusion. This case report demonstrates the application of qBOLD to topographically differentiate the metabolic states within the tumor and its surrounding region. Combined observations of qBOLD parameters inclusive of OEF and CVBVF revealed a heterogenous characteristic of cellularity and vascular distribution in a meningioma tumor, and a uniformly low region of CVBVF for the low-grade glioma indicative of hypo-perfusion.

5. Conclusions

The Quantitative BOLD (qBOLD) method exhibits remarkable versatility, finding applications across a wide range of fields, with a particular emphasis on neurology. It plays a pivotal role in facilitating the assessment of cerebral oxygenation by researchers and healthcare professionals in diverse scenarios. Its utility extends beyond the evaluation of brain tumors, encompassing conditions such as ischemic stroke, where impaired blood flow directly impacts the determination of Oxygen Extraction Fraction, and neurodegenerative diseases characterized by shifts in oxygen utilization patterns.

Moreover, the ongoing progress in qBOLD methodology and MRI technology has led to substantial advancements in terms of accuracy and sensitivity. Innovations in MRI sequences and post-processing techniques have significantly enhanced the precision of OEF estimation.

Conflicts of interest

The authors declare no conflict of interest.

References

1. Jokivarsi K, Chen YI, Kwong K, et al. Blood flow and oxygen extraction as biomarkers for activated brown adipose tissue. Journal of Nuclear Medicine 2012; 53(s1): 408.
2. Branca RT, Zhang L, Warren WS, et al. In vivo noninvasive detection of brown adipose tissue through intermolecular zero-quantum MRI. PloS One. 2013; 8(9): e74206.
3. Yoo H, Baia GS, Smith JS, et al. Expression of the hypoxia marker carbonic anhydrase 9 is associated with anaplastic phenotypes in meningiomas. Clinical Cancer Research 2007; 13(1): 68–75. doi: 10.1158/1078-0432.ccr-06-1377
4. Welford SM, Giaccia AJ. Hypoxia and senescence: The impact of oxygenation on tumor suppression. Can Hypoxia Promote Tumor Initiation. Molecular Cancer Research 2011; 9(5): 538–544. doi: 10.1158/1541-7786.mcr-11-0065
5. Phillips RM. Targeting the hypoxic fraction of tumours using hypoxia-activated prodrugs. Cancer Chemotherapy and Pharmacology 2016; 77(3): 441–457. doi: 10.1007/s00280-015-2920-7
6. Pugh CW, Ratcliffe PJ. The von Hippel-Lindau tumor suppressor, hypoxia-inducible factor-1 (HIF-1) degradation, and cancer pathogenesis. Seminars in Cancer Biology 2003; 13(1): 83–89. doi: 10.1016/j.cell.2004.08.025
7. Welter M. A Theoretical Model of Vascularized Tumors: Simulation of Blood Vessel Network Remodeling, Interstitial Fluid Flow and Oxygenation [PhD thesis]. Saarland University; 2015.
8. Chen TC, Zee CS, Miller CA, et al. Magnetic resonance imaging and pathological correlates of meningiomas. Neurosurgery 1992; 31(6): 1015–1022. doi: 10.1227/00006123-199212000-00005
9. Beaney RP, Brooks DJ, Leenders KL, et al. Blood flow and oxygen utilisation in the contralateral cerebral cortex of patients with untreated intracranial tumours as studied by positron emission tomography, with observations on the effect of decompressive surgery. Journal of Neurology, Neurosurgery & Psychiatry 1985; 48(4): 310–319. doi: 10.1136/jnnp.48.4.310
10. Nakayama Y, Tanaka A, Kumate S, Yoshinaga S. Cerebral blood flow in normal brain tissue of patients with intracranial tumors. Neurologia Medico-Chirurgica 1996; 36(10): 709–715. doi: 10.2176/nmc.36.709
11. Lebrun-Grandié P, Baron JC, Soussaline F, et al. Coupling between regional blood flow and oxygen utilization in the normal human brain: A study with positron tomography and oxygen 15. Archives of Neurology 1983; 40(4): 230–236. doi: 10.1001/archneur.1983.04050040060010
12. Cho J, Lee J, An H, et al. Cerebral oxygen extraction fraction (OEF): Comparison of challenge-free gradient echo QSM+qBOLD (QQ) with 15O PET in healthy adults. Journal of Cerebral Blood Flow & Metabolism 2021; 41(7): 1658–1668. doi: 10.1177/0271678x20973951
13. Bammer R, Keeling SL, Augustin M, et al. Improved diffusion-weighted single-shot echo-planar imaging (EPI) in stroke using sensitivity encoding (SENSE). Magnetic Resonance in Medicine 2001; 46(3): 548–554. doi: 10.1002/mrm.1226
14. Turner R, Le Bihan D, Scott Chesnicks A. Echo-planar imaging of diffusion and perfusion. Magnetic Resonance in Medicine 1991; 19(2): 247–253. doi: 10.1002/mrm.1910190210
15. Deichmann R, Gottfried JA, Hutton C, Turner R. Optimized EPI for fMRI studies of the orbitofrontal cortex. Neuroimage 2003; 19(2): 430–441.
16. Bolar DS, Rosen BR, Sorensen AG, Adalsteinsson E. Quantitative imaging of extraction of oxygen and tissue consumption (QUIXOTIC) using venular-targeted velocity-selective spin labeling. Magnetic Resonance in Medicine 2011; 66(6): 1550–1562. doi: 10.1002/mrm.22946
17. Hoge RD. Calibrated FMRI. Neuroimage 2012; 62(2): 930–937. doi: 10.1016/j.neuroimage.2012.02.022
18. Gauthier CJ, Hoge RD. Magnetic resonance imaging of resting OEF and CMRO (2) using a generalized calibration model for hypercapnia and hyperoxia. Neuroimage 2012; 60(2): 1212–1225. doi: 10.1016/j.neuroimage.2011.12.056
19. Wise RG, Harris AD, Stone AJ, Murphy K. Measurement of OEF and absolute CMRO 2: MRI-based methods using interleaved and combined hypercapnia and hyperoxia. Neuroimage 2013; 83: 135–147. doi: 10.1016/j.neuroimage.2013.06.008
20. Bulte DP, Kelly M, Germuska M, et al. Quantitative measurement of cerebral physiology using respiratory-calibrated MRI. Neuroimage 2012; 60(1): 582–591. doi: 10.1016/j.neuroimage.2011.12.017

21. He X, Yablonskiy DA. Quantitative BOLD: Mapping of human cerebral deoxygenated blood volume and oxygen extraction fraction: Default state. Magnetic Resonance in Medicine 2007; 57(1): 115–126. doi: 10.1002/mrm.21108
22. Wang X, Sukstanskii AL, Yablonskiy DA. Optimization strategies for evaluation of brain hemodynamic parameters with qBOLD technique. Magnetic Resonance in Medicine 2013; 69(4): 1034–1043. doi: 10.1002/mrm.24338
23. Wehrli FW, Fan AP, Rodgers ZB, et al. Susceptibility-based time-resolved whole-organ and regional tissue oximetry. NMR in Biomedicine 2017; 30(4): 10. doi: 10.1002/nbm.3495
24. Fan AP, Benner T, Bolar DS, et al. Phase-based regional oxygen metabolism (PROM) using MRI. Magnetic Resonance in Medicine 2012; 67(3): 669–678. doi: 10.1002/mrm.23050
25. Jiang D, Lu H. Cerebral oxygen extraction fraction MRI: Techniques and applications. Magnetic Resonance in Medicine 2022; 88(2): 575–600. doi: 10.1002/mrm.29272
26. Yablonskiy DA, Sukstanskii AL, He X. Blood oxygenation level-dependent (BOLD)-based techniques for the quantification of brain hemodynamic and metabolic properties—Theoretical models and experimental approaches. NMR Biomedicine 2013; 26(8): 963–986. doi: 10.1002/nbm.2839
27. Ulrich X, Yablonskiy DA. Separation of cellular and BOLD contributions to T2* signal relaxation. Magnetic Resonance Medicine 2016; 75(2): 606–615. doi: 10.1002/mrm.25610
28. Yablonskiy DA, Sukstanskii AL, Luo J, Wang X. Voxel spread function method for correction of magnetic field inhomogeneity effects in quantitative gradient-echo-based MRI. Magnetic Resonance Medicine 2013; 70(5): 1283–1292. doi: 10.1002/mrm.24585
29. Horten BC, Urich H, Rubinstein LJ, Montague SR. The angioblastic meningioma: A reappraisal of a nosological problem: Light-, electron-microscopic, tissue, and organ culture observations. Journal of the Neurological Sciences. 1977; 31(3): 387-410.
30. Liu G, Chen ZY, Ma L, et al. Intracranial hemangiopericytoma: MR imaging findings and diagnostic usefulness of minimum ADC values. Journal of Magnetic Resonance Imaging. 2013; 38(5): 1146-1151.
31. Perry A, Brat DJ. Practical surgical neuropathology a diagnostic approach. Churchill Livingstone Elsevier, Philadelphia. 2010; 185-217.
32. Miyake K, Ogawa D, Okada M, et al. Usefulness of positron emission tomographic studies for gliomas. Neurologia Medico-Chirurgica 2016; 56(7): 396–408. doi: 10.2176/nmc.ra.2015-0305
33. Rodgers ZB, Detre JA, Wehrli FW. MRI-based methods for quantification of the cerebral metabolic rate of oxygen. Journal of Cerebral Blood Flow and Metabolism 2016; 36(7): 1165–1185. doi: 10.1177/0271678X16643090
34. Christen T, Bouzat P, Pannetier N, et al. Tissue oxygen saturation mapping with magnetic resonance imaging. Journal of Cerebral Blood Flow and Metabolism 2014; 34(9): 1550–1557. doi: 10.1038/jcbfm.2014.116